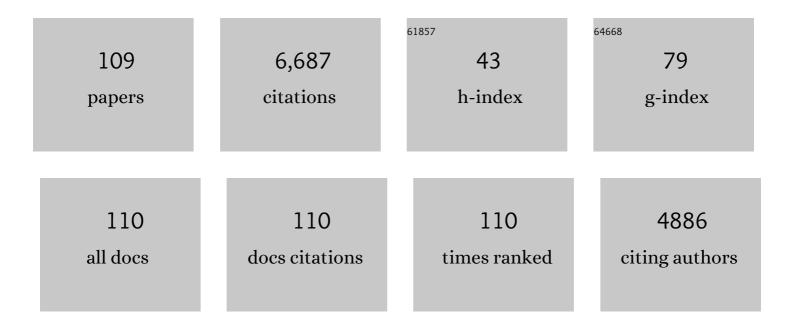
## Qin-Qin Liu

List of Publications by Year in descending order

Source: https://exaly.com/author-pdf/2255463/publications.pdf Version: 2024-02-01



#	Article	IF	CITATIONS
1	Interfacial active-site-rich 0D Co3O4/1D TiO2 p-n heterojunction for enhanced photocatalytic hydrogen evolution. Chemical Engineering Journal, 2022, 428, 131338.	6.6	133
2	Construction of g-C3N4 nanotube/Ag3PO4 S-scheme heterojunction for enhanced photocatalytic oxygen generation. Ceramics International, 2022, 48, 2169-2176.	2.3	22
3	Highly metallic Co-doped MoS2 nanosheets as an efficient cocatalyst to boost photoredox dual reaction for H2 production and benzyl alcohol oxidation. Carbon, 2022, 188, 70-80.	5.4	54
4	Dual plasmonic Au and TiN cocatalysts to boost photocatalytic hydrogen evolution. Chemosphere, 2022, 291, 132987.	4.2	20
5	Rational Design of 0D/2D WO 3 /g  3 N 4 Zâ€scheme Hybrid for Improving Photocatalytic Dye Degradation. ChemistrySelect, 2022, 7, .	0.7	2
6	Doping-induced metal–N active sites and bandgap engineering in graphitic carbon nitride for enhancing photocatalytic H2 evolution performance. Chinese Journal of Catalysis, 2022, 43, 421-432.	6.9	59
7	Plasmonic TiN nanobelts assisted broad spectrum photocatalytic H2 generation. Journal of Materials Science and Technology, 2022, 116, 1-10.	5.6	31
8	Carbon hollow spheres as cocatalyst of Cu-doped TiO2 nanoparticles for improved photocatalytic H2 generation. Rare Metals, 2022, 41, 2063-2073.	3.6	23
9	A review on photocatalytic systems capable of synchronously utilizing photogenerated electrons and holes. Rare Metals, 2022, 41, 2387-2404.	3.6	40
10	A 2D bimetallic Ni–Co hydroxide monolayer cocatalyst for boosting photocatalytic H <sub>2</sub> evolution. Chemical Communications, 2022, 58, 6180-6183.	2.2	12
11	Efficient photocatalytic hydrogen evolution coupled with benzaldehyde production over 0D Cd0.5Zn0.5S/2D Ti3C2 Schottky heterojunction. Journal of Advanced Ceramics, 2022, 11, 1117-1130.	8.9	48
12	Facile synthesis of ZnCd-MOF/Ag3PO4 heterojunction for highly efficient photocatalytic oxygen evolution. Research on Chemical Intermediates, 2022, 48, 2821-2835.	1.3	3
13	Enhanced photocatalytic antibacterial performance by hierarchical TiO2/W18O49 Z-scheme heterojunction with Ti3C2Tx-MXene cocatalyst. Chemical Engineering Journal, 2022, 447, 137369.	6.6	41
14	Construction of a ZnIn <sub>2</sub> S <sub>4</sub> /Au/CdS Tandem Heterojunction for Highly Efficient CO <sub>2</sub> Photoreduction. Inorganic Chemistry, 2022, 61, 11207-11217.	1.9	24
15	Construction of LSPR-enhanced 0D/2D CdS/MoO3â^' S-scheme heterojunctions for visible-light-driven photocatalytic H2 evolution. Chinese Journal of Catalysis, 2021, 42, 87-96.	6.9	254
16	Multiphase phosphide cocatalyst for boosting efficient photocatalytic H2 production and enhancing the stability. Ceramics International, 2021, 47, 1414-1420.	2.3	13
17	Oxygen Vacancies Induced Plasmonic Effect for Realizing Broadâ€Spectrumâ€Driven Photocatalytic H <sub>2</sub> Evolution over an Sâ€Scheme CdS/W <sub>18</sub> O <sub>49</sub> Heterojunction. ChemNanoMat, 2021, 7, 44-49.	1.5	44
18	Internal electric field induced S–scheme heterojunction MoS2/CoAl LDH for enhanced photocatalytic hydrogen evolution. Journal of Colloid and Interface Science, 2021, 585, 470-479.	5.0	154

#	Article	IF	CITATIONS
19	Unraveling the Roles of Hot Electrons and Cocatalyst toward Broad Spectrum Photocatalytic H <sub>2</sub> Generation of g <sub>3</sub> N <sub>4</sub> Nanotube. Solar Rrl, 2021, 5, 2000504.	3.1	54
20	Band Engineering and Morphology Control of Oxygen-Incorporated Graphitic Carbon Nitride Porous Nanosheets for Highly Efficient Photocatalytic Hydrogen Evolution. Nano-Micro Letters, 2021, 13, 48.	14.4	43
21	Construction of S-scheme MnO2@CdS heterojunction with core–shell structure as H2-production photocatalyst. Rare Metals, 2021, 40, 2381-2391.	3.6	60
22	Polyethyleneimine induced highly dispersed Ag nanoparticles over g-C3N4 nanosheets for efficient photocatalytic and antibacterial performance. Ceramics International, 2021, 47, 8528-8537.	2.3	17
23	Unraveling the Roles of Hot Electrons and Cocatalyst toward Broad Spectrum Photocatalytic H <sub>2</sub> Generation of g <sub>3</sub> N <sub>4</sub> Nanotube. Solar Rrl, 2021, 5, 2170063.	3.1	14
24	The origin of enhanced photocatalytic activity in g-C3N4/TiO2 heterostructure revealed by DFT calculations. Journal of Colloid and Interface Science, 2021, 593, 133-141.	5.0	59
25	Lattice-Matched CoP/CoS <sub>2</sub> Heterostructure Cocatalyst to Boost Photocatalytic H <sub>2</sub> Generation. Inorganic Chemistry, 2021, 60, 12506-12516.	1.9	40
26	The synergistic effect of P doping and Ni(II) electron cocatalyst boosting photocatalytic H2-evolution activity of g-C3N4. Ceramics International, 2021, 47, 23386-23395.	2.3	11
27	Hot-electron-assisted S-scheme heterojunction of tungsten oxide/graphitic carbon nitride for broad-spectrum photocatalytic H2 generation. Chinese Journal of Catalysis, 2021, 42, 1478-1487.	6.9	99
28	Designing 0D/2D CdS nanoparticles/g-C3N4 nanosheets heterojunction as efficient photocatalyst for improved H2-evolution. Surfaces and Interfaces, 2021, 26, 101312.	1.5	22
29	Construction of UiO-66/Bi4O5Br2 Type-II Heterojunction to Boost Charge Transfer for Promoting Photocatalytic CO2 Reduction Performance. Frontiers in Chemistry, 2021, 9, 804204.	1.8	8
30	An overview of graphene oxide supported semiconductors based photocatalysts: Properties, synthesis and photocatalytic applications. Journal of Molecular Liquids, 2020, 297, 111826.	2.3	91
31	Build-in electric field induced step-scheme TiO2/W18O49 heterojunction for enhanced photocatalytic activity under visible-light irradiation. Ceramics International, 2020, 46, 23-30.	2.3	99
32	In situ fabrication of 1D CdS nanorod/2D Ti3C2 MXene nanosheet Schottky heterojunction toward enhanced photocatalytic hydrogen evolution. Applied Catalysis B: Environmental, 2020, 268, 118382.	10.8	429
33	Enhanced n→Ĩ€* electron transition of porous P-doped g-C3N4 nanosheets for improved photocatalytic H2 evolution performance. Ceramics International, 2020, 46, 8444-8451.	2.3	61
34	Revealing and accelerating interfacial charge carrier dynamics in Z-scheme heterojunctions for highly efficient photocatalytic oxygen evolution. Applied Catalysis B: Environmental, 2020, 268, 118445.	10.8	69
35	Synergistic effect of Co(II)-hole and Pt-electron cocatalysts for enhanced photocatalytic hydrogen evolution performance of P-doped g-C3N4. Chinese Journal of Catalysis, 2020, 41, 72-81.	6.9	114
36	Insights into the Effect of Reactive Oxygen Species Regulation on Photocatalytic Performance via Construction of a Metal-Semiconductor Heterojunction. Journal of Nanoscience and Nanotechnology, 2020, 20, 3478-3485.	0.9	5

#	Article	IF	CITATIONS
37	A latest overview on photocatalytic application of g-C3N4 based nanostructured materials for hydrogen production. International Journal of Hydrogen Energy, 2020, 45, 337-379.	3.8	175
38	Mechanistic insights into charge carrier dynamics in MoSe2/CdS heterojunctions for boosted photocatalytic hydrogen evolution. Materials Today Physics, 2020, 15, 100261.	2.9	23
39	Oxygen doped g <sub>3</sub> N <sub>4</sub> with nitrogen vacancy for enhanced photocatalytic hydrogen evolution. Chemistry - an Asian Journal, 2020, 15, 3456-3461.	1.7	69
40	Construction 0D TiO2 nanoparticles/2D CoP nanosheets heterojunctions for enhanced photocatalytic H2 evolution activity. Journal of Materials Science and Technology, 2020, 56, 196-205.	5.6	126
41	Effects of oxygen defects on electronic band structures and dopant migration in Sn-doped TiO2 by density functional studies. Chemical Physics Letters, 2020, 754, 137732.	1.2	11
42	Recent advances in MXenes supported semiconductors based photocatalysts: Properties, synthesis and photocatalytic applications. Journal of Industrial and Engineering Chemistry, 2020, 85, 1-33.	2.9	107
43	A 3D nitrogen-doped graphene aerogel for enhanced visible-light photocatalytic pollutant degradation and hydrogen evolution. RSC Advances, 2020, 10, 12423-12431.	1.7	18
44	Copper matrix thermal conductive composites with low thermal expansion for electronic packaging. Ceramics International, 2020, 46, 18019-18025.	2.3	25
45	Porous Ni5P4 as a promising cocatalyst for boosting the photocatalytic hydrogen evolution reaction performance. Applied Catalysis B: Environmental, 2020, 275, 119144.	10.8	194
46	Fabrication of dual direct Z-scheme g-C3N4/MoS2/Ag3PO4 photocatalyst and its oxygen evolution performance. Applied Surface Science, 2019, 463, 9-17.	3.1	145
47	The synergetic effect of carbon nanotubes and MoS2 as co-catalysts for enhancing the photocatalytic oxygen evolution of Ag3PO4. Ceramics International, 2019, 45, 21120-21126.	2.3	27
48	Built-in electric field induced CeO2/Ti3C2-MXene Schottky-junction for coupled photocatalytic tetracycline degradation and CO2 reduction. Ceramics International, 2019, 45, 24146-24153.	2.3	152
49	Enhancement in photocatalytic activity of CO2 reduction to CH4 by 0D/2D Au/TiO2 plasmon heterojunction. Applied Surface Science, 2019, 493, 1142-1149.	3.1	83
50	Constructing 0D FeP Nanodots/2D g  3 N 4 Nanosheets Heterojunction for Highly Improved Photocatalytic Hydrogen Evolution. ChemCatChem, 2019, 11, 6310-6315.	1.8	33
51	Construction of Ti3C2 MXene/O-doped g-C3N4 2D-2D Schottky-junction for enhanced photocatalytic hydrogen evolution. Ceramics International, 2019, 45, 24656-24663.	2.3	113
52	Probing supramolecular assembly and charge carrier dynamics toward enhanced photocatalytic hydrogen evolution in 2D graphitic carbon nitride nanosheets. Applied Catalysis B: Environmental, 2019, 256, 117867.	10.8	137
53	Oxamide-modified g-C3N4 nanostructures: Tailoring surface topography for high-performance visible light photocatalysis. Chemical Engineering Journal, 2019, 374, 1064-1075.	6.6	218
54	Light-induced ZnO/Ag/rGO bactericidal photocatalyst with synergistic effect of sustained release of silver ions and enhanced reactive oxygen species. Chinese Journal of Catalysis, 2019, 40, 691-702.	6.9	53

#	Article	IF	CITATIONS
55	Localized Surface Plasmon Resonance Induced Band Gap Regulation Governing the Excellent Photocatalytic Performance of Ag/g-C3N4 Heterostructure. Journal of Nanoscience and Nanotechnology, 2019, 19, 5582-5590.	0.9	8
56	Supramolecular precursor strategy for the synthesis of holey graphitic carbon nitride nanotubes with enhanced photocatalytic hydrogen evolution performance. Nano Research, 2019, 12, 2385-2389.	5.8	192
57	Accelerating photocatalytic hydrogen evolution and pollutant degradation by coupling organic co-catalysts with TiO2. Chinese Journal of Catalysis, 2019, 40, 380-389.	6.9	105
58	Remarkable Enhancement in Solar Oxygen Evolution from MoSe <sub>2</sub> /Ag <sub>3</sub> PO <sub>4</sub> Heterojunction Photocatalyst via In Situ Constructing Interfacial Contact. ACS Sustainable Chemistry and Engineering, 2019, 7, 8466-8474.	3.2	92
59	Unveiling the origin of boosted photocatalytic hydrogen evolution in simultaneously (S, P,) Tj ETQq1 1 0.784314 84-94.	4 rgBT /Ov 10.8	erlock 10 Tf 300
60	Two-dimensional Sn2Ta2O7 nanosheets as efficient visible light-driven photocatalysts for hydrogen evolution. Rare Metals, 2019, 38, 397-403.	3.6	49
61	Interfacial optimization of g-C3N4-based Z-scheme heterojunction toward synergistic enhancement of solar-driven photocatalytic oxygen evolution. Applied Catalysis B: Environmental, 2019, 244, 240-249.	10.8	295
62	Sc2W3O12/Cu composites with low thermal expansion coefficient and high thermal conductivity for efficient cooling of electronics. Journal of Alloys and Compounds, 2019, 779, 108-114.	2.8	31
63	Scandium (21Sc). World Scientific Series in Nanoscience and Nanotechnology, 2019, , 153-156.	0.1	0
64	3D reduced graphene oxide aerogel-mediated Z-scheme photocatalytic system for highly efficient solar-driven water oxidation and removal of antibiotics. Applied Catalysis B: Environmental, 2018, 232, 562-573.	10.8	231
65	Optical tuning by the self-assembly and disassembly of chain-like plasmonic superstructures. National Science Review, 2018, 5, 128-130.	4.6	23
66	Construction of Ternary rGO/Ag2CO3/AgBr Heterostructured Photocatalyst for Improved Photocatalytic Activity and Stability. Journal of Nanoscience and Nanotechnology, 2018, 18, 7867-7872.	0.9	1
67	Bifunctional Material with Organic Pollutant Removing and Antimicrobial Properties: Graphene Aerogel Decorated with Highly Dispersed Ag and CeO <sub>2</sub> Nanoparticles. ACS Sustainable Chemistry and Engineering, 2018, 6, 16907-16919.	3.2	23
68	Highly Active, Superstable, and Biocompatible Ag/Polydopamine/g-C <sub>3</sub> N <sub>4</sub> Bactericidal Photocatalyst: Synthesis, Characterization, and Mechanism. ACS Sustainable Chemistry and Engineering, 2018, 6, 14082-14094.	3.2	76
69	N,S-Atom-coordinated Co <sub>9</sub> S <sub>8</sub> trinary dopants within a porous graphene framework as efficient catalysts for oxygen reduction/evolution reactions. Dalton Transactions, 2018, 47, 14992-15001.	1.6	37
70	Porous graphene doped with Fe/N/S and incorporating Fe <sub>3</sub> O <sub>4</sub> nanoparticles for efficient oxygen reduction. Catalysis Science and Technology, 2018, 8, 5325-5333.	2.1	33
71	Ecofriendly and environment-friendly synthesis of size-controlled silver nanoparticles/graphene composites for antimicrobial and SERS actions. Applied Surface Science, 2018, 457, 1000-1008.	3.1	30
72	Insights Into Highly Improved Solar-Driven Photocatalytic Oxygen Evolution Over Integrated Ag3PO4/MoS2 Heterostructures. Frontiers in Chemistry, 2018, 6, 123.	1.8	19

#	Article	IF	CITATIONS
73	Porous MoP network structure as co-catalyst for H2 evolution over g-C3N4 nanosheets. Applied Surface Science, 2018, 462, 822-830.	3.1	120
74	Anchoring metal-organic framework nanoparticles on graphitic carbon nitrides for solar-driven photocatalytic hydrogen evolution. Applied Surface Science, 2018, 455, 403-409.	3.1	108
75	Dual Z-scheme g-C3N4/Ag3PO4/Ag2MoO4 ternary composite photocatalyst for solar oxygen evolution from water splitting. Applied Surface Science, 2018, 456, 369-378.	3.1	196
76	Fast and green synthesis of silver nanoparticles/reduced graphene oxide composite as efficient surface-enhanced Raman scattering substrate for bacteria detection. Monatshefte Für Chemie, 2017, 148, 1155-1163.	0.9	16
77	Construction of carbon nitride and MoS2 quantum dot 2D/0D hybrid photocatalyst: Direct Z-scheme mechanism for improved photocatalytic activity. Chinese Journal of Catalysis, 2017, 38, 2160-2170.	6.9	165
78	One-step synthesis of recycled 3D CeVO <sub>4</sub> /rGO composite aerogels for efficient degradation of organic dyes. RSC Advances, 2016, 6, 85779-85786.	1.7	16
79	Influence of doping and solid solution formation on photocatalytic activity of ZrW2O8with cubic structure. Materials Technology, 2016, , 1-7.	1.5	1
80	Band gap and morphology engineering of TiO <sub>2</sub> by silica and fluorine co-doping for efficient ultraviolet and visible photocatalysis. RSC Advances, 2016, 6, 63117-63130.	1.7	30
81	Fabrication of 3D CeVO 4 /graphene aerogels with efficient visible-light photocatalytic activity. Ceramics International, 2016, 42, 10487-10492.	2.3	50
82	In-situ synthesis of Sc2W3O12/YSZ ceramic composites with controllable thermal expansion. Ceramics International, 2015, 41, 8267-8271.	2.3	14
83	Synthesis, photocatalytic performance and negative thermal expansion property of nanorods ZrMo2â^'x V x O8â^'x/2 with cubic structure. Journal of Sol-Gel Science and Technology, 2015, 76, 279-288.	1.1	2
84	One-pot synthesis of g-C3N4/V2O5 composites for visible light-driven photocatalytic activity. Applied Surface Science, 2015, 358, 188-195.	3.1	94
85	Synthesis and characterization of sol–gel derived ZrV2O7 fibers with negative thermal expansion property. Journal of Sol-Gel Science and Technology, 2014, 72, 502-510.	1.1	8
86	Preparation and Thermal Expansion Property of ZrWMoO8/Cu Composite. Rare Metal Materials and Engineering, 2014, 43, 1798-1802.	0.8	2
87	Structural, negative thermal expansion and photocatalytic properties of ZrV2O7: a comparative study between fibers and powders. Materials Characterization, 2014, 96, 63-70.	1.9	10
88	Fabrication of In 2 O 3 @In 2 S 3 core–shell nanocubes for enhanced photoelectrochemical performance. Journal of Power Sources, 2014, 247, 915-919.	4.0	54
89	Synthesis and tunable thermal expansion properties of Sc2â^xYxW3O12 solid solutions. Ceramics International, 2014, 40, 8195-8199.	2.3	10
90	Influence of W doped ZrV2O7 on structure, negative thermal expansion property and photocatalytic performance. Applied Surface Science, 2014, 313, 41-47.	3.1	24

Qin-Qin Liu

#	Article	IF	CITATIONS
91	Effect of acids on the morphology and negative thermal expansion analysis of ZrW2O8 powders prepared by the hydrothermal method. Ceramics International, 2013, 39, 165-170.	2.3	13
92	Defect-controlled ZnO nanorod arrays for enhanced photoelectrochemical performance. Inorganic Chemistry Communication, 2013, 30, 182-186.	1.8	15
93	Development of low thermal expansion Sc <sub>2</sub> (WO <sub>4</sub> ) <sub>3</sub> containing composites. Materials Technology, 2012, 27, 388-392.	1.5	15
94	Preparation, characterization and photocatalytic activities of ZrWMoO8/Ag composites with core–shell structure. Applied Surface Science, 2012, 261, 593-597.	3.1	10
95	Preparation and characterization of negative thermal expansion Sc2W3O12/Cu core–shell composite. Ceramics International, 2012, 38, 541-545.	2.3	38
96	Fabrication of negative thermal expansion ZrMo2O8 film by sol–gel method. Materials Science and Engineering B: Solid-State Materials for Advanced Technology, 2012, 177, 263-268.	1.7	9
97	Influence of fabrication method on the structure and thermal expansion property of ZrWMoO8 and its composites. Journal of Materials Science, 2011, 46, 1253-1258.	1.7	4
98	Abnormal positive thermal expansion in Mo substituted ZrW2O8. Physica B: Condensed Matter, 2011, 406, 3458-3464.	1.3	4
99	Preparation of TiO <sub>2</sub> pillared layered titanate photocatalyst by sol intercalation method. Materials Technology, 2010, 25, 39-41.	1.5	4
100	Preparation of Negative Thermal Expansion ZrW2O8 Powders and Its Application in Polyimide/ZrW2O8 Composites. Journal of Materials Science and Technology, 2010, 26, 665-668.	5.6	33
101	Synthesis of negative thermal expansion materials ZrW2â^'xMoxO8 (0≤â‰⊉) using hydrothermal method. Ceramics International, 2009, 35, 441-445.	2.3	10
102	Study on the synthesis of Al2W2MoO12 by a simple stearic acid route and its negative thermal expansion property. Ceramics International, 2009, 35, 3131-3134.	2.3	9
103	Influence of sodium dodecyl benzene sulfonate (SDBS) on the morphology and negative thermal expansion property of ZrW2O8 powders synthesized by hydrothermal method. Journal of Alloys and Compounds, 2009, 481, 668-672.	2.8	30
104	Morphology control and negative thermal expansion in cubic ZrWMoO <sub>8</sub> powders. Physica Status Solidi (B): Basic Research, 2008, 245, 2477-2482.	0.7	9
105	Preparation of rutile TiO2 nanofibers by TiO2 sol intercalation of ultrafine layered titanate. Materials Letters, 2007, 61, 1855-1858.	1.3	13
106	Preparation and characterization of ZrWMoO8 powders with different morphologies using hydrothermal method. Journal of Materials Science, 2007, 42, 2528-2531.	1.7	10
107	Preparation and characterization of ZrWMoO8 powders with different morphologies. Frontiers of Chemistry in China: Selected Publications From Chinese Universities, 2007, 2, 359-363.	0.4	0
108	Preparation and Negative Thermal Expansion Property of ZrWMoO <sub>8</sub> . Advanced Materials Research, 0, 177, 245-248.	0.3	0

#	Article	IF	CITATIONS
109	Engineering MoS 2 Cocatalysts as Active Sites over Porous Pâ€Doped g  3 N 4 Nanosheets to Enhance Photocatalytic Hydrogen Production. Physica Status Solidi - Rapid Research Letters, 0, , 2000513.	1.2	6